J. Chem. Sci. Vol. 123, No. 5, September 2011, pp. 577–592.

Ru^{4+} ion in CeO_2 ($Ce_{0.95}Ru_{0.05}O_{2-\delta}$): A non-deactivating, non-platinum catalyst for water gas shift reaction

PREETAM SINGH, N MAHADEVAIAH, SANJIT K PARIDA and M S HEGDE*
Solid State and Structural Chemistry Unit, Indian Institute of Science, Bangalore 560012, India
e-mail: mshegde@sscu.iisc.ernet.in

MS received 4 February 2011; revised 6 April 2011; accepted 11 May 2011

Abstract. Hydrogen is a clean energy carrier and highest energy density fuel. Water gas shift (WGS) reaction is an important reaction to generate hydrogen from steam reforming of CO. A new WGS catalyst, $Ce_{1-x}Ru_xO_{2-\delta}$ ($0 \leq x \leq 0.1$) was prepared by hydrothermal method using melamine as a complexing agent. The Catalyst does not require any pre-treatment. Among the several compositions prepared and tested, $Ce_{0.95}Ru_{0.05}O_{2-\delta}$ (5% Ru^{4+} ion substituted in CeO_2) showed very high WGS activity in terms of high conversion rate (20.5 μmol.g^{-1}.s^{-1} at 275°C) and low activation energy (12.1 kcal/mol). Over 99% conversion of CO to CO_2 by H_2O is observed with 100% H_2 selectivity at $\geq$ 275°C. In presence of externally fed CO_2 and H_2 also, complete conversion of CO to CO_2 was observed with 100% H_2 selectivity in the temperature range of 305–385°C. Catalyst does not deactivate in long duration on/off WGS reaction cycle due to absence of surface carbon and carbonate formation and sintering of Ru. Due to highly acidic nature of Ru^{4+} ion, surface carbonate formation is also inhibited. Sintering of noble metal (Ru) is avoided in this catalyst because Ru remains in Ru^{4+} ionic state in the $Ce_{1-x}Ru_xO_{2-\delta}$ catalyst.

Keywords. WGS reaction; Ru^{4+} ion in CeO_2; Pt catalyst; H_2 selectivity.

1. Introduction

Industrially, hydrogen is produced by steam reforming of hydrocarbon followed by water gas shift (WGS) reaction. WGS reaction is a crucial step to remove CO from the synthesis gas which is produced from reforming of hydrocarbons. The reaction is written as:

$$CO + H_2O \rightarrow CO_2 + H_2 \qquad \Delta H = -41.1\,kJ/mol, \quad \Delta G = -28.6kJ/mol. \tag{1}$$

Gasification of bio-mass or wood is another way to produce syngas, also known as wood gas.[1,2] WGS reaction can also be effectively employed to generate hydrogen directly from wood gas provided high conversion rate is achieved and long term activity of a WGS catalyst is retained.

For the production of hydrogen via WGS reaction, an efficient catalyst is required. There are two types of WGS catalysts which are commercially used: (i) high temperature shift catalyst and (ii) low temperature shift catalyst. Fe_2O_3–Cr_2O_3 mixed oxide is a high temperature shift catalyst. It works under high partial pressure or concentration of CO and catalytic performance decreases under high CO_2 partial pressures or low CO partial pressure. CuO–ZnO–Al_2O_3 mixed oxide is a well-known low temperature shift catalyst. It works under low partial pressure or concentration of CO but it is highly susceptible to poisoning, and requires long pre-treatment process. In recent times, cerium dioxide-based WGS catalysts have attracted increasing attention as an alternative to Cu/ZnO and Fe_2O_3–Cr_2O_3 based catalysts due to its oxygen storage property (OSC).[3–7] Pt supported ceria and non-metallic Pt and Au in 10–20% La^{3+} doped CeO_2 have shown high activity towards WGS reaction.[8–12] High activity of Pt/CeO_2 catalyst is attributed to redox mechanism where CO is adsorbed on Pt site and H_2O is activated on the support. Due to high oxygen storage property of ceria, CO adsorbed on metal site gets oxidized to CO_2 by ceria, followed by oxidation of reduced ceria with water to produce hydrogen.[4,5] However, deactivation of the Pt/CeO_2 catalyst under working conditions (both long time runs at certain temperatures and shutdown–startup cycles) is observed. Deactivation of the Pt/CeO_2 catalyst is due to (i) over reduction of the CeO_2 support, (ii) surface carbonate and formate formation and (iii) sintering of Pt metal.[13–15] To overcome the over reduction of ceria, some less reducible supports such as TiO_2 and ZrO_2 are investigated as possible alternatives to CeO_2. Pt/ZrO_2 is stable under WGS

*For correspondence

reaction, but it showed lower activity than Pt/CeO_2.[16] Pt metal supported on TiO_2 also acts as WGS catalyst, but the catalyst deactivates due to sintering of Pt metal.[17–19] Further, due to high cost of Pt, high loading of Pt, the catalyst will be economically prohibitive.[20] Na promoted Pt/TiO_2 catalysts showed better performance near equilibrium WGS reaction condition. Reason for high activity is attributed to absence of sintering of Pt metal particles due to addition of Na, possibly through the interactions of $Pt–NaO_x–TiO_2$.[21]

1–2% Pt^{2+} ion substituted CeO_2, TiO_2, and $Ce_{1-x}Ti_xO_2$ have shown better performance for WGS reaction because sintering of Pt is avoided due to the presence of Pt in the ionic form in these noble metal ionic catalysts.[22] Pt ion substituted TiO_2 in the form of $Ti_{0.99}Pt_{0.01}O_{2-\delta}$ showed high CO conversion by water and catalyst does not get deactivated under long usage of on/off WGS reaction cycle due to absence of surface carbonate and formate formation. Surface carbonate and formate formation over this catalyst is inhibited due to the acidic nature of Ti^{4+} ion. 2 atom% Pt^{2+} ion substituted $Ce_{0.8}Sn_{0.2}O_2$ viz. $Ce_{0.78}Sn_{0.2}Pt_{0.02}O_{2-\delta}$ also showed high conversion for hydrogen generation via water–gas shift reaction. Catalyst also does not deactivate due to absence of carbonate formation over this catalyst.[23]

We have recently demonstrated that up to 10% of Ru^{4+} ion can be substituted for Ce^{4+} ion in CeO_2 by hydrothermal method using melamine as a complexing agent.[24] $Ce_{1-x}Ru_xO_{2-\delta}$ ($0 \leq x \leq 0.1$) nanocrystallites showed high OSC as well as three-way catalytic activity at much lower temperature than Pt^{2+} and Pd^{2+} ion substituted CeO_2.[24] Even in absence of externally fed O_2, high degree of CO oxidation was observed via utilization of lattice oxygen of $Ce_{1-x}Ru_xO_{2-\delta}$. It means lattice oxygen is activated in this compound and the oxide ion vacancies are replenished by the feed oxygen. Hence $Ce_{1-x}Ru_xO_{2-\delta}$ can be a good catalyst for WGS reaction. Here we show that 5% Ru^{4+} ion substituted CeO_2 ($Ce_{0.95}Ru_{0.05}O_{2-\delta}$) is a good WGS catalyst.

2. Experimental

2.1 *Synthesis*

Synthesis and structure of Ru^{4+} ion substituted CeO_2 catalyst is discussed in details in our earlier report.[24] $Ce_{1-x}Ru_xO_{2-\delta}$ ($x = 0.02$, 0.05 and 0.1) were synthesized by hydrothermal method using melamine as a complexing agent. For the preparation of $Ce_{1-x}Ru_xO_{2-\delta}$ ($x = 0.02$, 0.05 and 0.1) catalysts, starting materials ceric ammonium nitrate ($Ce(NH_4)_2(NO_3)_6$) ($\geq$ 98%, Sigma Aldrich), $RuCl_3.xH_2O$ (99.98%, Sigma Aldrich) and melamine (99%, Sigma Aldrich) were taken in the ratio of $1-x : x : 2$. In a typical synthesis of $Ce_{0.95}Ru_{0.05}O_{2-\delta}$, 2.375 mM of $Ce(NH_4)_2(NO_3)_6$ was dissolved in 20 ml of distilled water and 0.135 mM of $RuCl_3.xH_2O$(Aldrich) was dissolved in 5 ml of water. Both the solutions were mixed in 5.0 mM of melamine ($C_3N_6H_6$) solution made in 25 ml of hot water (75°C). The solution turned into a gel. The resulting gel was stirred for ten minutes in warm condition (75°C). The gel was transferred into three autoclave bombs of 20 ml capacity with 75% filling and they were placed in a pre-heated hot air oven at 200°C for 24 h. The black coloured precipitate obtained after 24 h of hydrothermal treatment was filtered and dried in hot air oven at 120°C for 6 h. 5 atom% Ru metal impregnated on CeO_2 catalyst was also prepared by reducing the $RuCl_3.H_2O$ solution by hydrazine hydrate (98%, Sigma Aldrich) over CeO_2 nanocrystallites. For this purpose 1 g of CeO_2 nanocrystallite of 8–10 nm made by hydrothermal[24] method was mixed in 50 ml of distilled water. Then 0.061 g of $RuCl_3.H_2O$ was added in the mixture and stirred it for 10 min. Then slowly Hydrazine hydrate solution was added drop-by-drop in the mixture to reduce the $RuCl_3.H_2O$ to ru metal. Mixture was further stirred to 30 min. The black coloured mixture was filtered and dried at 110°C for 5 h. The resulting dried solid precipitate was further reduced in H_2 at 200°C to avoid presence of any traces of ruthenium oxide in the catalyst.

X-ray diffraction (XRD) pattern of powders were recorded in a Phillips X'Pert diffractometer using Cu Kα radiation at scan rate of $0.2°min^{-1}$ with 0.01° step size in the 2θ range between 10 and 90°. Structures were refined by Rietveld method, using FullProf-fp2k program.[25] For transmission electron microscopy (TEM), toluene dispersion of the sample was dropped onto the carbon coated Cu grids and images were recorded with FEI Technai 20 at 200 kV. X-ray photoelectron spectra (XPS) of selected samples were recorded in a Thermo Scientific Multilab 2000 instrument using Al Kα X-ray at 150 W. Binding energies reported here are with reference to C(1s) at 284.5 eV and are accurate within $\pm$ 0.1 eV. FT-IR spectra of the samples were recorded with Perkin-Elmer FT-IR Spectroscopy Spectrum 1000.

2.2 *Catalysis study*

Reactions were carried out at atmospheric pressure in a fixed bed quartz micro-reactor. Powder catalyst was

pressed and granules of 40–80 mesh size were made. Those pressed granules of the catalysts were loaded in the micro reactor of length 30 and 0.4 cm internal diameter for WGS reaction study. Calibrated 10% CO/N_2 procured from Chemix, Bangalore, India, was used as CO source. Reactions were carried out as a function of temperature. 5 cc/min CO and 30 cc/min H_2O vapor were passed along with N_2 keeping the total gas flow at 130 cc/min over 200 mg of catalyst to achieve the GHSV of 55900 h^{-1}. H_2O was injected by syringe pump and heated at 120°C in stainless-steel tube before mixing it in to the input/feed gas. Water vapor flow was kept 30 cc/min. Gaseous products obtained from the WGS reaction were analysed by online gas chromatograph (prog. GC, Mayura Analytical Pvt. Ltd., India) equipped with flame ionization and thermal conductivity detectors. All hydrocarbons were separated by Haysep-A column having mesh size 80/100 and dimensions 2 m × 1/8 inch. Detection is done by FID detector. CO and CO_2 were converted in to methane prior to the detection in FID by the methanator having a Ru catalyst on molecular-sieve. H_2 was detected using TCD.

The water vapor in the output gas stream was first condensed in water condenser before passing in to GC for analysis in all the studies. The total dry gas (after condensing H_2O vapor from output stream) flow sent for analysis in GC was 100 cc/min. In GC, N_2 was used as carrier gas. CO, CO_2 and hydrocarbons were detected by flame ionization detector (FID). H_2 was detected by thermal conductivity detector (TCD) in GC. Methanizer is used to detect the CO and CO_2 by FID in the GC. WGS studies were also carried out in high CO_2 and H_2-rich environment with a gas composition close to wood gas composition. For this study, WGS reaction was carried out over 200 mg of catalyst with gas mixture, 5 cc/min CO, 10 cc/min H_2, 10 cc/min CO_2 and 30 cc/min H_2O vapor balance with N_2 keeping the total gas flow 130 cc/min and GHSV 55900 h^{-1}. WGS reaction was also carried out with gas composition, 5 cc/min CO, 40 cc/min H_2 and 30 cc/min H_2O vapor balance in N_2 keeping the total gas flow and GHSV same. Volume of CO, CO_2, H_2 and other by-products of the reaction (CH_4, other hydrocarbons, HCHO, HCOOH and CH_3OH) were measured independently in GC in the product stream. Only CO_2, H_2 and methane were formed in WGS reaction with Ru^{4+} ion substituted CeO_2 and Ru metal impregnated CeO_2 catalysts according to the reaction given below:

$$CO + H_2O \rightarrow CO_2 + H_2, \tag{2}$$

and

$$CO + 3H_2 \rightarrow CH_4 + H_2O. \tag{3}$$

Signal (area under the peak) of CO_2, H_2 and CH_4 in GC were calibrated against the signal for known volume of 10% CO_2/N_2, 10% H_2/N_2 and 5% CH_4/N_2 flowing with same speed (100 cc/min). For each reaction, conversion of CO, balance of CO_2, H_2 and CH_4 and their selectivity(s) were calculated. Conversion and selectivity(s) of the reaction were calculated from the following equations:

$$\text{CO conversion} = \left(F_{CO\,(in)} - F_{CO(out)}\right)/F_{CO(in)}, \tag{4}$$

$$S_{H2} = F_{H2}/(F_{H2} + 2F_{CH4} + F_{H2O}), \tag{5}$$

$$S_{CH4} = F_{CH4}/(F_{H2} + F_{CH4} + F_{H2O}). \tag{6}$$

$F_{x(in)}$ is input flow of gas (x) and $Fx_{(out)}$ is flow of gas (x) in product stream. The spent catalysts were tested for further WGS reaction without any pre-treatment.

Reverse WGS reaction was also carried out both in presence and absence of externally fed H_2O gas. Reaction was carried out with gas composition 5 cc/min CO_2, 5 cc/min H_2 and 30 cc/min H_2O balance in N_2 keeping total flow 130 cc/min over 200 mg of catalyst. Reaction was also carried out with gas composition 5 cc/min CO_2, and 5 cc/min H_2 balance in N_2 keeping total flow 130 cc/min (in absence of feed H_2O) over 200 mg of catalyst.

3. Results and discussion

3.1 *WGS study*

%CO, CO_2 and H_2 concentration as a function of temperature with $Ce_{0.98}Ru_{0.02}O_{2-\delta}$ (2% Ru^{4+} ion in CeO_2) catalyst is shown (figure 1a). Complete conversion of CO to CO_2 by H_2O was observed at 465°C. H_2 formation was also consistent with CO_2 formation and CO conversion. $[H_2]/[CO_2]$ ratio in product stream was also ∼ 1 and no methane was detected in the product stream within the detection limit of 3–5 ppm in GC. Thus, almost 100% H_2 selectivity was observed with this catalyst. % CO, CO_2 and H_2 concentration as a function of temperature with $Ce_{0.95}Ru_{0.05}O_{2-\delta}$ (5% Ru^{4+} ion in CeO_2) catalyst is shown (figure 1b). Compared to $Ce_{0.98}Ru_{0.02}O_{2-\delta}$, almost complete CO conversion (∼99.9%) was observed at much lower temperature (275°C) with $Ce_{0.95}Ru_{0.05}O_{2-\delta}$ and residual CO peak

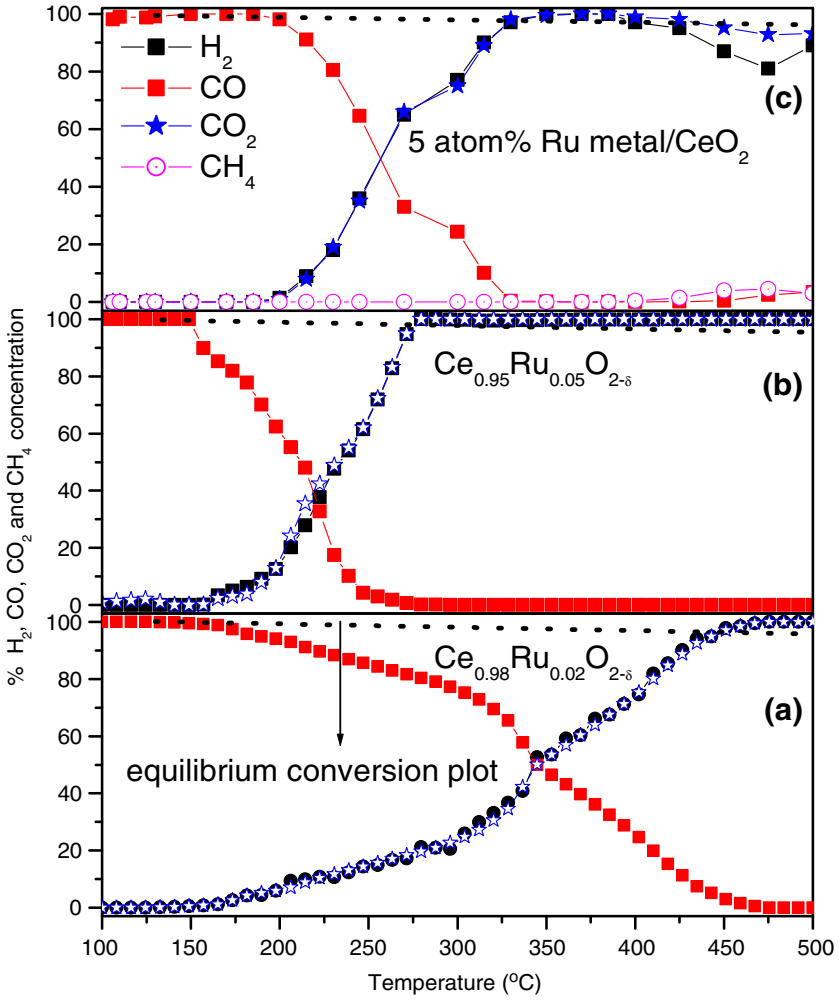

Figure 1. %CO, H_2, CO_2 and CH_4 concentration plot as a function of temperature with gas composition 5 cc/min CO, 30 cc/min H_2O balance in N_2 (total flow, 130 cc/min) over 200 mg of (**a**) $Ce_{0.98}Ru_{0.02}O_{2-\delta}$, (**b**) $Ce_{0.95}Ru_{0.05}O_{2-\delta}$ and (**c**) 5 atom% Ru metal impregnated on CeO_2 catalyst. %Equilibrium CO conversion to CO_2 is plotted by dotted line in each case.

could not be detected in GC in the detection limit of 3–5 ppm. No trace of methane was formed with this catalyst and $[H_2]/[CO_2]$ was ~ 1 in the product stream in the temperature range of 120 to 500°C. Other possible by-products of the reaction such as CH_3OH, H_2CO, CH_4 and other hydrocarbons were not detected in the product stream. Thus, the catalyst shows $\sim$ 100% selectivity for H_2 formation under the WGS reaction condition given above.

Even though equilibrium conversion in WGS reaction is limited by exothermic nature of the reaction and at higher temperature decrease in conversion is expected. By taking the thermodynamic consideration, a simpler equation for Keq is given by Moe.[26]

$$K\text{eq} = \exp(4577.8/T - 4.33), \qquad (7)$$

where Keq is equilibrium constant for WGS reaction and T is reaction temperature in Kelvin. For the input gas composition 5 cc/min CO and 30 cc/min H_2O balance in N_2 (total flow = 130 cc/min) the equilibrium CO conversion to CO_2 will be $\sim$ 96.2% at 500°C. However $\sim$ 100% conversion is observed at this temperature with this catalyst. Equilibrium CO conversion to CO_2 is plotted for each WGS reaction.

For comparison, WGS study was also carried with 5 atom% Ru metal impregnated on CeO_2 catalyst. WGS reaction was carried out with gas composition 5 cc/min CO, 30 cc/min H_2O balance in N_2 keeping total flow 130 cc/min over 200 mg of the catalyst (figure 1c) and $\sim$ 99.5% CO to CO_2 conversion was observed at 330°C with this Ru metal impregnated on CeO_2 catalyst. However with Ru metal impregnated CeO_2 catalyst at higher

temperature, CO conversion decreases and methane formation was also observed. For example at 500°C, ~94% CO is converted to CO_2, 3% converted to CH_4 and remaining 3% CO unreacted. Thus with Ru metal impregnated on CeO_2 catalyst, complete conversion of CO is not achieved at higher temperature. Only with $Ce_{0.95}Ru_{0.05}O_{2-\delta}$, almost complete (~ 99.9%) conversion of CO to CO_2 with 100% H_2 selectivity was observed at 275°C and this conversion is sustained even up to 500°C.

%CO, CO_2, H_2 and CH_4 concentration as a function of temperature with $Ce_{0.9}Ru_{0.1}O_{2-\delta}$ (10% Ru^{4+} ion in CeO_2) catalyst is shown (figure 2a). $Ce_{0.9}Ru_{0.1}O_{2-\delta}$ showed higher CO conversion at lower temperature compared to other two compositions, but at higher temperature methane was formed along with H_2 and CO_2. Only 87% CO is converted to CO_2 by H_2O at 275°C and rest 13% was converted to methane by the spontaneous H_2 produced in WGS reaction. % H_2 and CH_4 selectivity with this catalyst is plotted (figure 2b). One possible reason for methane formation activity is the possibility of Ru^{4+} ion reduction to Ru^0 under the reducing condition of CO and H_2. Ru metal is known for methane formation. Reducibility of Ru^{4+} ion increases with increasing Ru^{4+} ion concentrations. Accordingly in 10% Ru^{4+} ion substituted CeO_2, methane is formed. However with 5% Ru^{4+} ion, methane formation activity is drastically Reduced. Up to 250°C, H_2 selectivity of the catalyst was 100% but at higher temperatures H_2 selectivity decreases. In the temperature range of 275 to 350°C, H_2 selectivity was ~62% and CH_4 selectivity was ~9%. H_2 selectivity was ~100% with 2% and 5% Ru ion substituted CeO_2 namely $Ce_{0.98}Ru_{0.02}O_{2-\delta}$ and $Ce_{0.95}Ru_{0.05}O_{2-\delta}$ in the temperature range of 120–500°C. $Ce_{0.95}Ru_{0.05}O_{2-\delta}$ showed superior activity compared to other two compositions and 5 atom% Ru metal impregnated CeO_2 catalyst. Therefore, we focused our study mainly on the WGS activity of 5% Ru ion in CeO_2, $Ce_{0.95}Ru_{0.05}O_{2-\delta}$ catalyst.

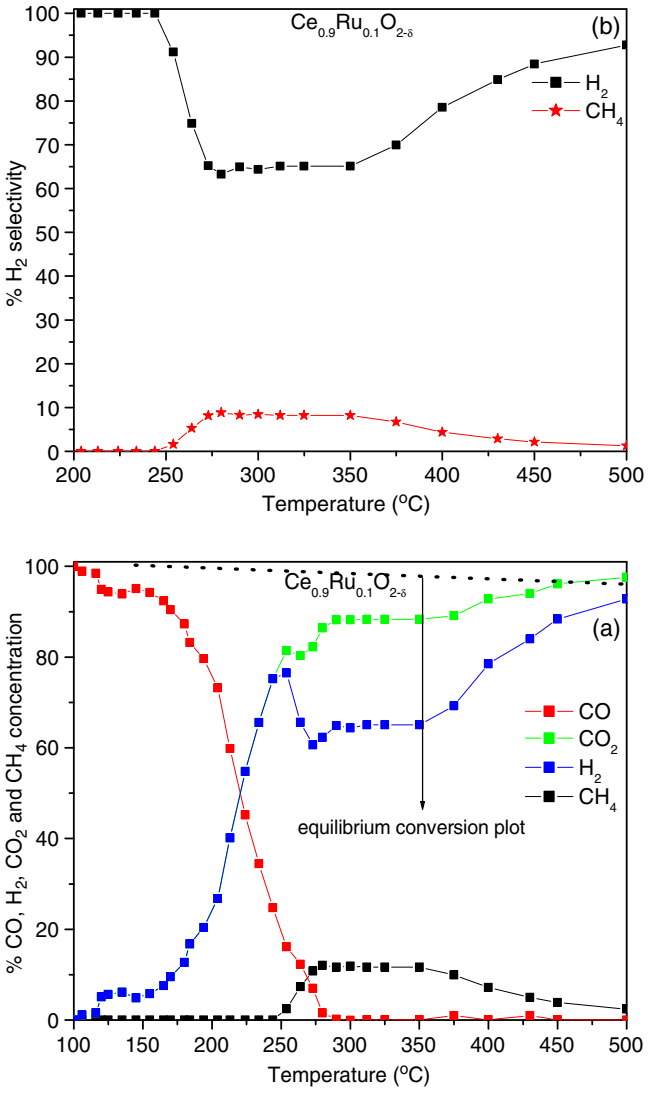

Figure 2. (**a**) %CO, H_2, CO_2 and CH_4 plot and (**b**) %H_2 and CH_4 selectivity as a function of temperature with gas composition 5 cc/min CO, 30 cc/min H_2O balance in N_2 (total flow, 130 cc/min) with $Ce_{0.9}Ru_{0.1}O_{2-\delta}$ catalyst. %Equilibrium CO conversion to CO_2 is plotted by dotted line in figure 2a.

To study the role of H_2O concentration in reaction (1), WGS reaction was carried out with H_2O vapor flow rates of 15 cc/min, 30 cc/min and 40 cc/min, keeping the CO flow at 5 cc/min and the weight of the catalyst same for all the reaction. CO conversion plots with 15 cc/min and 30 cc/min of H_2O vapor pressure are shown (figures 3a and b). At lower temperature, almost same CO conversions were observed with both the flow rates of H_2O. Almost complete conversion of CO to CO_2 occurs at 275°C with water vapor flow of 30 and at 305°C with H_2O vapor flow of 15 cc/min. The conversion sustained up to 500°C with both the flow of H_2O vapor. However, equilibrium CO conversion to CO_2 with feed gas composition 5 cc/min CO and 15 cc/min H_2O balance in N_2 keeping total flow 130 cc/min will be ~ 91.7% at 500°C. Plot for CO conversion to CO_2 with 40 cc/min of H_2O vapor flow is not shown because it showed almost similar profile like 30 cc/min of water vapor flow and complete conversion was also observed at ~275°C. Thus with CO: H_2O molar flow ratio of 1:6, highest conversion was observed. That is why in all the studies CO: H_2O flow ratio was kept 1:6.

To determine the actual rate and activation energy of the reaction with this catalyst, WGS reactions were carried out with different weight of the catalyst ranging from 25 to 200 mg, keeping total gas flow and GHSV

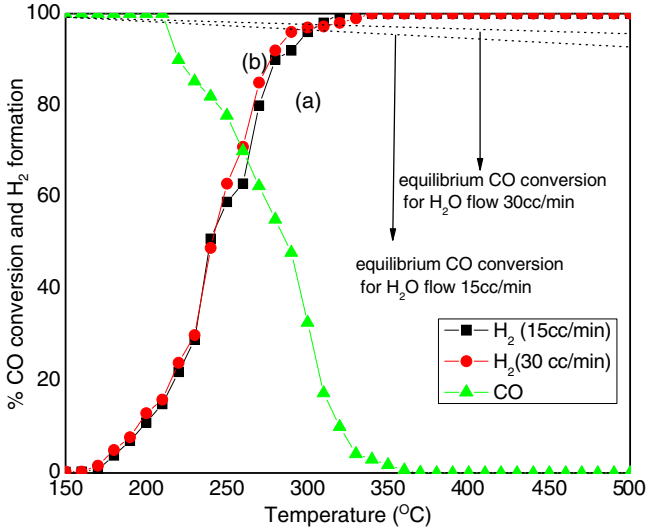

Figure 3. %H_2 formation plot in WGS reaction at a gas hourly space velocity (GHSV) 55900 h^{-1} over $Ce_{0.95}Ru_{0.05}O_{2-\delta}$ catalyst with CO flow of 5 cc/min and water flow (**a**) of 15 cc/min and (**b**) 30 cc/min (balance in N_2 and total flow in both case is 130 cc/min). %Equilibrium CO conversion to CO_2 is plotted by dotted line in each case.

same. To keep GHSV same, total bed length of catalyst were kept same by mixing the required amount of silica granules of 40–80 mess size along with catalyst granules. Fractional conversion (x) vs W/F plot (figure 4a) and rate of the WGS reaction was derived from the equation,

$$\text{Rate(r)} = \text{(F.x)/W or x/(W/F)}, \qquad (8)$$

where x is fractional conversion, w is weight of the catalyst and F is gas flow. Rate (r) vs. temperature T (°C) (figure 4b) and ln(r) vs. 1000/T(K) plot is shown in the inset of figure 4b. Rate of CO conversion to CO_2 by H_2O was found as high as 20.5 μmol.g^{-1}.s^{-1} at 275°C. Activation energy was calculated form Ln(r) vs 1/T plot and it was found 12.1 kcal/mol. $Ce_{0.95}Ru_{0.05}O_2$ was found superior in terms of high conversion rates and low activation energy compared to other catalysts reported in literature and a comparison of WGS activity of different catalysts is given (table 1).

Hydrogen gas obtained from reforming reactions contains large volume of CO and CO_2 along with H_2. Thus a WGS catalyst should be active or able to retain high conversion of CO to CO_2 and H_2 formation even in the presence of high concentration/partial pressure of H_2 and CO_2. To see the viability of this $Ce_{0.95}Ru_{0.05}O_{2-\delta}$ catalyst, WGS reactions were carried out in two different conditions: (i) in presence of large volumes of

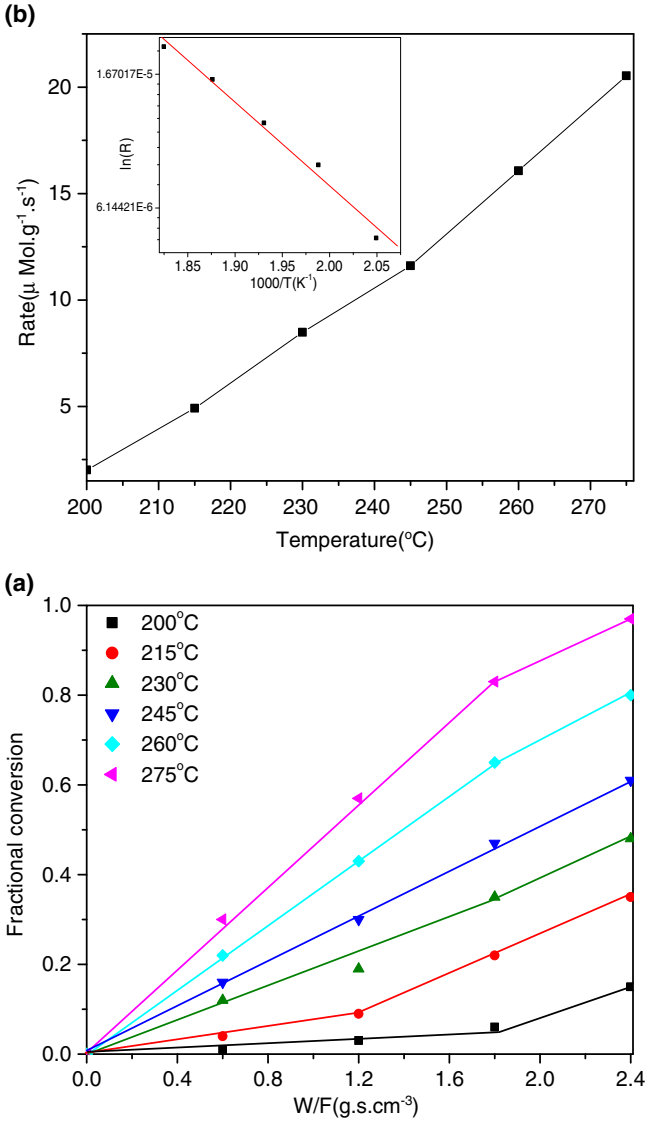

Figure 4. (**a**) Fractional CO conversion (x) vs. W/F plot for different weight of $Ce_{0.95}Ru_{0.05}O_{2-\delta}$ and (**b**) rate(r) vs. temperature plot and inset of the (**b**) shows Ln(r) vs. 1000/T (K^{-1}) plot derived from fractional conversion (x) vs. W/F plot in WGS reaction with gas composition 5 cc/min CO, 30 cc/min H_2O balance in N_2 (total flow, 130 cc/min).

externally fed H_2 and (ii) in presence of both externally fed H_2 and CO_2. In the first case, WGS reaction was carried out with a gas composition of 5 cc/min CO, 40 cc/min H_2 and 30 cc/min H_2O vapor balance with N_2 over 200 mg of the catalyst. Even in presence of such a high volume of H_2 complete CO conversion to CO_2 with 100% H_2 selectivity was observed at 335°C (figure 5a). In presence of externally fed H_2, complete CO conversion to CO_2 or H_2 formation temperature was shifted to higher temperature (335°C) compared to CO conversion to H_2 at 275°C in absence of externally fed H_2.

Table 1. Comparison of rate and activation for WGS reaction with different catalysts.

Compound	%CO	%H_2O	%H_2	%CO_2	max conversion (%) & T max (°C)	Rate μmol $g^{-1}s^{-1}$ at Temp (°C)	Turn over Frequency (s^{-1}) at temp (°C)	$E_a$kcal/mol	Reference
0.5%Pt/CeO_2	3	7.5			≥ 99.5, 300				14
0.5% Pt/$Ce_{0.5}Ti_{0.5}O_2$	3	7.5			≥ 99.5, 300				14
0.5%Pt/TiO_2	3	7.5			≥ 99.5, 300				14
1.5%Pt10%La/CeO_2	11	26	26	7	≥ 99.5	1 (350)	0.015 (350)	18	13
2.7% Pt10%La/eO_2	11	26	26	7	≥ 99.5	1.5 (350)	0.011 (350)	18	13
3.7% Pt10%La/CeO_2	11	26	26	7	≥ 99.5	2 (350)	0.01 (350)	18	13
1%Pt/CeO_2	7	22	37	8.5		0.59 (200)	0.01 (200)		13
$Ti_{0.99}Pt_{0.01}O_{2-\delta}$	2	30	50		97, 310	12.9 (280)	0.104 (280)	10	22
$Ce_{0.78}Ti_{0.20}Pt_{0.02}O_{2-\delta}$	2	30			≥ 99.8, 360	14.5 (220)	0.109 (220)		22
$Ce_{0.78}Ti_{0.20}Pt_{0.02}O_{2-\delta}$	2	30	50		98, 355	7.54 (280)	0.058 (280)	13.5	22
$Ce_{0.98}Pt_{0.02}O_{2-\delta}$	2	30			≥ 99.8, 300	4.5 (220)	0.04 (220)		22
$Ce_{0.98}Pt_{0.02}O_{2-\delta}$	2	30	50		95, 400	6.62 (280)	0.06 (280)	15	22
$Ce_{0.78}Sn_{0.2}Pt_{0.02}O_{2-\delta}$	3.8	25	36			11.1 (300)	0.09 (300)	6.7	23
$Ce_{0.95}Ru_{0.05}O_{2-\delta}$	5	30			≥ 99.8, 275	20.5 (275)	0.08 (275)	12.1	Present work
$Ce_{0.95}Ru_{0.05}O_{2-\delta}$	5	30	10	10	≥ 99.8, 305	14.5 (275)	0.06 (275)	12.6	Present work
$Ce_{0.95}Ru_{0.05}O_{2-\delta}$	5	30	40		≥ 99.8, 335	9.85 (275)	0.04 (275)	13.5	Present work

Even in presence of 40% volume of externally fed H_2, methane formation was not observed and H_2 formation was 100% selective up to 500°C. Equilibrium CO conversion to CO_2 plot was also given in figure 5a and it should be ~ 72.3% at 500°C. Activation energy and rate of H_2 formation in this case was calculated by taking the data for conversion < 20% from figure 5a. Activation energy was found 13.5 kcal/mol and rate was found 9.85 mol.g^{-1}.s^{-1} at 275°C (table 1).

In the second condition, WGS reaction was carried with a gas composition of 5 cc/min CO, 10 cc/min CO_2, 10 cc/min H_2 and 30 cc/min H_2O vapor balance with N_2 over 200 mg of catalyst. Indeed complete conversion of CO to CO_2 by H_2O with 100% H_2 selectivity was observed in the temperature range of 305 to 380°C (figure 5b). Equilibrium CO conversion to CO_2 is also plotted (figure 5b) and it should be ~ 74.2% at 500°C. In our study also, methane formation was observed above 380°C (figure 5b) and CO conversion to CO_2 was decreasing at higher temperature. In the temperature window of 305 to 380°C, $Ce_{0.95}Ru_{0.05}O_{2-\delta}$ can function for CO oxidation to CO_2 by water to produce H_2 with 100% selectivity even in presence of excess or external/feed H_2 and CO_2 in the input stream. Rate and activation energy for H_2 formation were calculated by taking the data for conversion <20% from figure 5b. Activation energy was found 12.6 kcal/mol and H_2 formation rate was found 14.5 μmol.g^{-1}.s^{-1} at 275°C in this reaction condition (table 1).

Turnover frequency (TOF) of the catalyst is also compared with other catalysts. TOF is calculated form the equation:

$$\text{TOF} = \frac{\text{Rate (moles of } H_2\text{/g of catalyst/s)}}{\text{Moles of noble metal per g of catalyst}}.$$

Pt metal impregnated catalysts over ceria based supports have TOF in the range of 0.01 s^{-1}.[13] Ionically substituted Pt in CeO_2, $Ce_{1-x}Ti_xO_2$, $Ce_{1-x}Sn_xO_2$ and TiO_2 has shown TOF in the range of 0.04–0.1 s^{-1}.[22,23] The present catalyst ($Ce_{0.95}Ru_{0.05}O_{2-\delta}$) has shown TOF of 0.08 s^{-1}. Temperature range of the conversion is ~ 300°C in most of the catalysts. Activation energy of ionically substituted catalysts are in the range of 10–12 kcal/mol of the catalyst. Activation energy of Pt metal impregnated over ceria based support catalysts are in the range of 18 kcal/mol. Thus $Ce_{0.95}Ru_{0.05}O_{2-\delta}$ catalyst is equally good to ionically Pt substituted catalysts. Thus a non-Pt catalyst presented here has shown high TOF and low activation energy. A comparison of rate, TOF and activation energy of different catalysts is given in table 1.

To see if there is any deactivation of catalyst under WGS reaction condition, long time on/off activity of catalyst was tested with a gas composition of 5 cc/min CO, 10 cc/min CO_2, 10 cc/min H_2 and 30 cc/min H_2O vapor balance with N_2 at 200°C, where ~ 15% conversion occurs and also at 350°C, where ~ 100% conversion

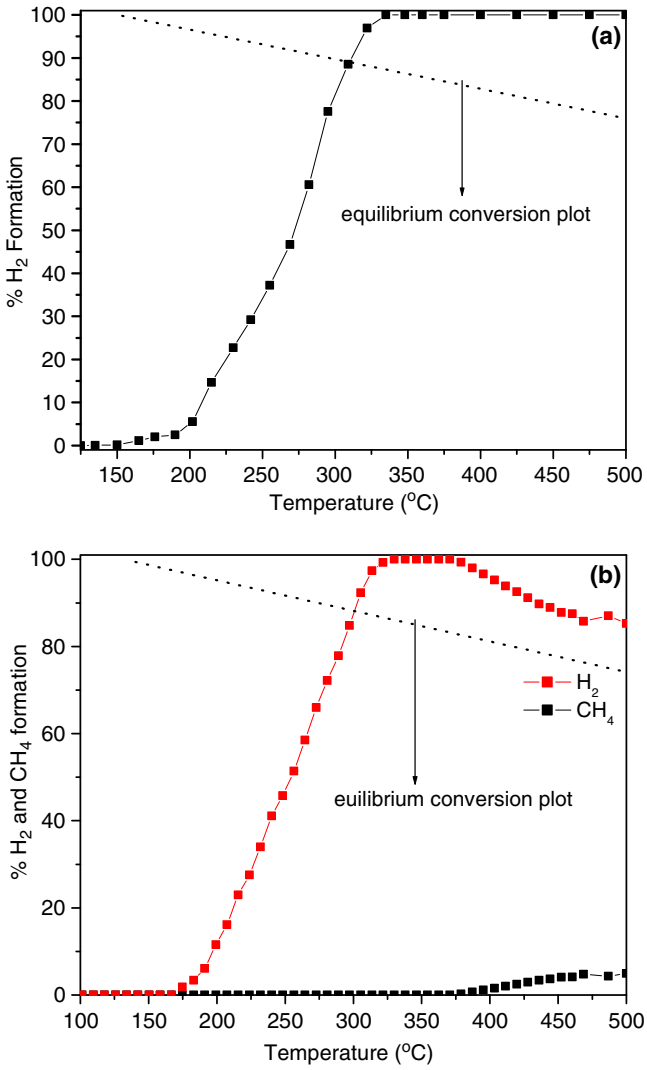

Figure 5. (**a**) % H_2 formation plot with 5 cc/min CO, 40 cc/min of H_2, 30 cc/min H_2O vapor balanced with N_2 keeping total flow 130 cc/min (GHSV = 55900 h^{-1}) over 200 mg of $Ce_{0.95}Ru_{0.05}O_{2-\delta}$ catalyst. (**b**) % H_2 and CH_4 formation plot with 5 cc/min CO, 10 cc/min of H_2, 10 cc/min CO_2 along with N_2 keeping total flow 130 cc/min (GHSV = 55900 h^{-1}) over 200 mg of $Ce_{0.95}Ru_{0.05}O_{2-\delta}$ catalyst. %Equilibrium CO conversion to CO_2 is plotted by dotted line in each case.

occurs for 4 consecutive cycles of 25 h (figures 6a, b). Reactions were stopped for 5 h in between two consecutive cycles. Reaction was restarted without any pretreatment of the catalyst. CO conversion was ~ 15% and equivalent amount of CO_2 and H_2 were formed at 200°C. There was no measurable change in %H_2, CO_2 and CO concentration with respect to time (figure 6a). There was no decrease in the activity of the catalyst with respect to time. Almost complete conversion of CO to CO_2 was observed with 100% H_2 selectivity for 100 h of reaction at 350°C and there was no measurable decrease in CO conversion to CO_2 and H_2 generation with respect to time. No trace of CH_4, CH_3OH, H_2CO or other hydrocarbons were observed at this temperature even after subjecting the catalyst under longer duration of reaction. Thus the catalyst ($Ce_{0.05}Ru_{0.05}O_{2-\delta}$) retained its activity for WGS reaction even under high partial pressure of externally fed H_2 and CO_2 and no deactivation of the catalyst was observed under long duration of reaction.

3.2 *Structural characterization*

To get an insight into the high activity and non-deactivating property of the $Ce_{0.95}Ru_{0.05}O_{2-\delta}$ catalyst, electronic structure and crystal structure of the catalyst before and after 100 h of on/off WGS reaction (spent catalyst) were examined by XRD, TEM, XPS and FT-IR. Powder XRD patterns of as prepared $Ce_{1-x}Ru_xO_{2-\delta}$ (x = 0.02, 0.05 and 0.1) are given in figures 7 (a–c) respectively. $Ce_{1-x}Ru_xO_{2-\delta}$ (x = 0.02, 0.05 and 0.1) crystallizes in cubic fluorite structure. No diffraction peaks corresponding to any of Ru, RuO_2, Ce-melamine, Ru-melamine complex phase was observed in powder XRD pattern. However, intense diffraction peaks for Ru metal were observed along with CeO_2 peaks in the powder XRD pattern of 5 atom% Ru metal impregnated on CeO_2 sample (figure 7d). Structural parameters of $Ce_{1-x}Ru_xO_{2-\delta}$ (x = 0.02, 0.05 and 0.1) obtained by Rietveld refinement of powder XRD data are summarized in table 2. In our earlier report, we have shown that up to 10% Ru^{4+} ion can be substituted for Ce^{4+} ion in CeO_2.[24]

Rietveld refined powder XRD pattern of as prepared $Ce_{0.95}Ru_{0.05}O_{2-\delta}$ and spent catalyst after 100 h of WGS reaction is shown in figures 8 (a, b). All the peaks were indexed to fluorite structure and peaks corresponding to RuO_2 or Ru metal impurities were not observed in the difference plot of the Rietveld refined powder XRD pattern of spent catalyst. It means Ru^{4+} ions were not separated out from the fluorite lattice during the WGS reaction. Structural parameters along with size of crystallites of spent catalyst are summarized (table 2). There was no noticeable change in the lattice parameter of the spent catalyst compared to freshly prepared catalyst.

Bright field and HRTEM image of spent $Ce_{0.95}Ru_{0.05}O_{2-\delta}$ catalyst are shown in figures 9 (a, b) respectively. Electron diffraction pattern was indexed to fluorite structure (inset of figure 9a). Enlarged view of lattice fringes of width 3.11 Å is shown in the inset of figure 9b. Bright field and HRTEM image of as synthesized $Ce_{0.95}Ru_{0.05}O_{2-\delta}$ catalyst is shown in figures 9

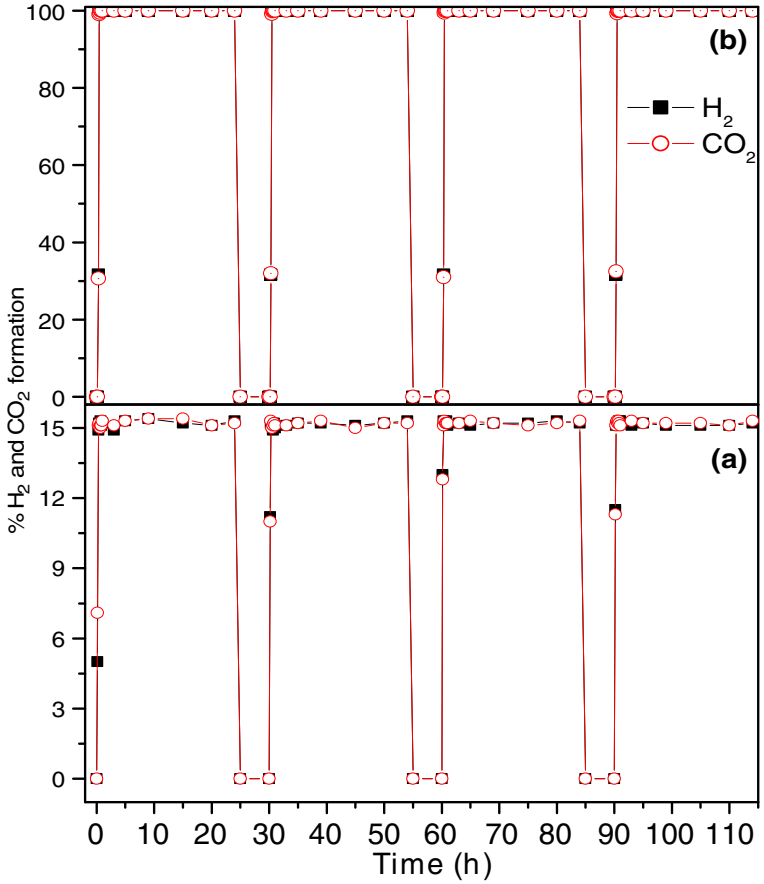

Figure 6. % H_2 and CO_2 formation plot in function of time on/off WGS reaction over 200 mg of $Ce_{0.95}Ru_{0.05}O_{2-\delta}$ at a space velocity of 55900 h^{-1} with gas flow of CO (5 cc/min), H_2 (10 cc/min), CO_2 (10 cc/min) and H_2O (30 cc/min) along with N_2 keeping total flow 130 cc/min (a) at 200°C and (b) 350°C.

(c, d) for comparison. Crystallite sizes are in 6–8 nm range for as synthesized catalyst and in the range of 8 ± 2 nm size for the spent catalyst after 100 h of on/off WGS reaction. Ring type electron diffraction pattern of as prepared catalyst (inset of figure 9c) was indexed to fluorite structure and lattice fringes were of 3.11 Å width (inset of figure 9d) which corresponds to d_{111} of $Ce_{0.95}Ru_{0.05}O_{2-\delta}$ lattice. Extensive search for RuO_2 or Ru metal particle were carried out by TEM study, but no impurities of corresponding phases were observed in electron diffraction pattern and HRTEM images of both the spent and as prepared $Ce_{0.95}Ru_{0.05}O_{2-\delta}$ catalysts. Thus the catalyst is stable under WGS reaction condition.

The oxidation states of Ru and Ce in $Ce_{0.95}Ru_{0.05}O_{2-\delta}$ in spent catalyst as well as in freshly prepared catalyst were determined by XPS. Ru (3d) spectrum of as prepared catalyst and the spent catalyst are shown in figures 10 (a, b) respectively. C(1 s) and Ru(3d) state occurs very close or near by in XPS. Thus the spectrum was resolved into C(1 s), Ru($3d_{5/2}$), and Ru($3d_{3/2}$) states and accordingly Ru($3d_{5/2}$) was observed at 281.4 eV and C(1 s) at 284.5 eV both in as prepared and spent catalyst. Binding energies of Ru($3d_{5/2}$) in Ru metal and RuO_2 are at 280.1 and 280.7 eV respectively.[27,28] Because RuO_2 is also metallic compound, the difference in Ru($3d_{5/2}$) binding energy for Ru^0 in Ru metal and Ru^{4+} state in RuO_2 is small.[29] Ru($3d_{5/2}$) binding energy at 281.4 eV in $Ce_{0.95}Ru_{0.05}O_{2-\delta}$ is higher than the binding energy of Ru($3d_{5/2}$) for Ru^{4+} state in RuO_2 and lower than the binding energy of Ru($3d_{5/2}$) for Ru^{6+} state in at 282.5 eV in RuO_3.[26] Binding energy of Ru^{4+}($3d_{5/2}$) in $Ce_{0.95}Ru_{0.05}O_{2-\delta}$ agrees well with the binding energy value for Ru^{4+} ion in $RuO_2.xH_2O$.[27,28] Therefore Ru was assigned to +4 oxidation state in both as prepared and spent catalyst ($Ce_{0.95}Ru_{0.05}O_{2-\delta}$). Thus there was no change in the oxidation state of Ru in the spent catalyst after 100 h of on/off WGS reaction.

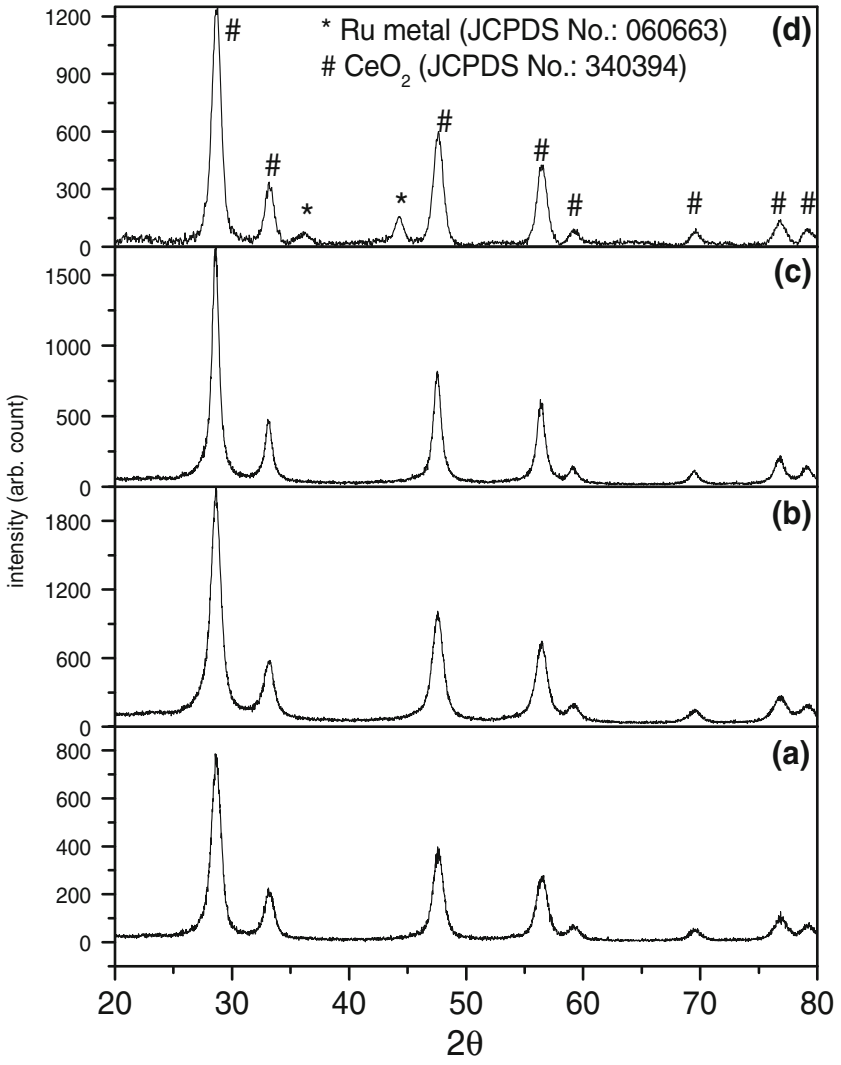

Figure 7. Powder XRD patterns of (**a**) $Ce_{0.98}Ru_{0.02}O_{2-\delta}$, (**b**) $Ce_{0.95}Ru_{0.05}O_{2-\delta}$, (**c**) $Ce_{0.9}Ru_{0.1}O_{2-\delta}$ and (**d**) 5 atom% Ru metal impregnated on CeO_2.

Table 2. Structural parameters of $Ce_{1-x}Ru_xO_{2-\delta}$ catalyst.

Compound	Condition	Lattice parameter	χ^2	R_B	R_f	Average crystallite sizes from rietveld refinement (TEM) nm
$Ce_{0.98}Ru_{0.02}O_{2-\delta}$	dried at 110°C for 2 h	5.411 (1)	1.19	1.78	1.16	6.5
$Ce_{0.95}Ru_{0.05}O_{2-\delta}$	dried at 110°C for 2 h	5.413 (1)	1.16	1.90	1.36	6.9 (8 ± 1)
$Ce_{0.90}Ru_{0.10}O_{2-\delta}$	dried at 110°C for 2 h	5.415 (2)	2.05	2.76	1.27	10.7 (9 ± 2)
$Ce_{0.95}Ru_{0.05}O_{2-\delta}$	after long duration of WGS reaction	5.415 (3)	1.35	2.11	1.45	10.9 (9 ± 2)

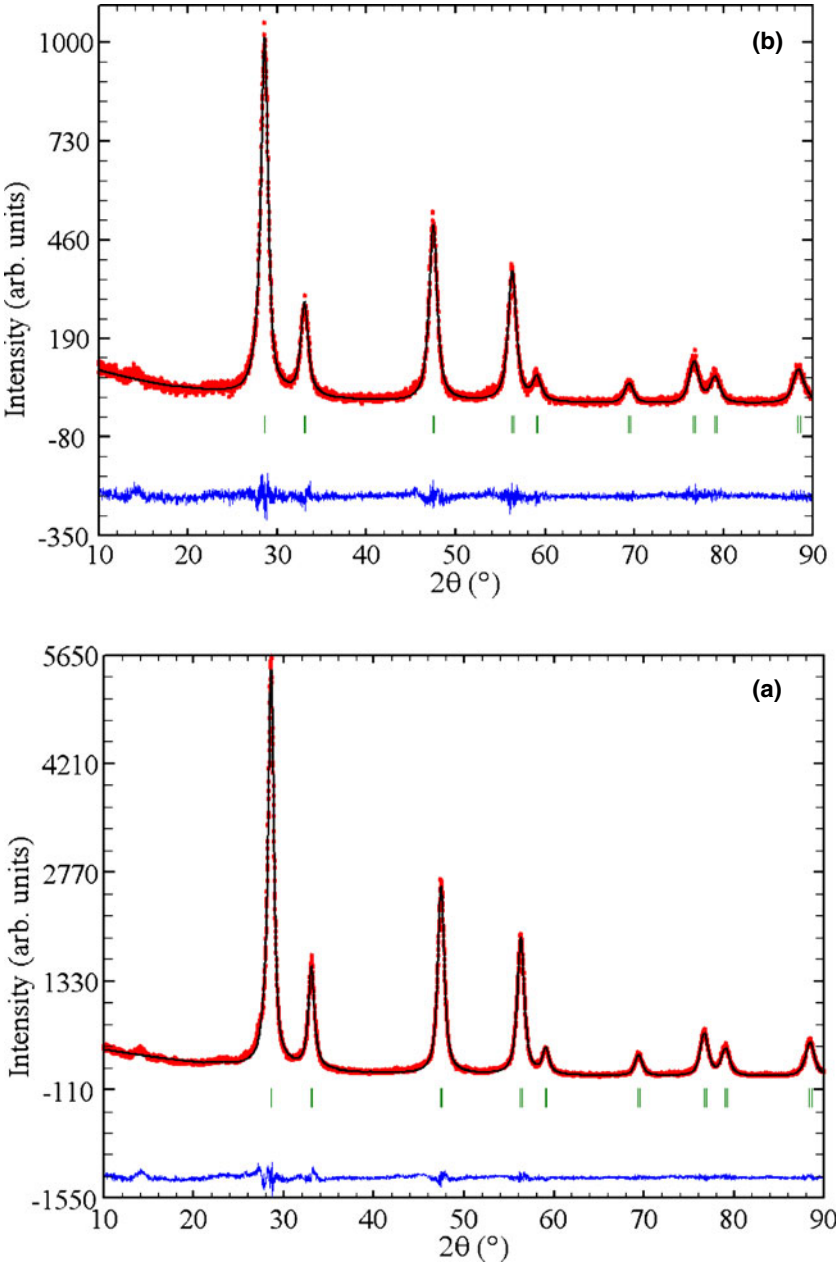

Figure 8. Rietveld refined powder XRD pattern of $Ce_{0.95}Ru_{0.05}O_{2-\delta}$ (**a**) freshly prepared and (**b**) spent catalyst after 100 h of on/off WGS reaction.

However in the case of Ru metal impregnated on CeO_2 sample, Ru($3d_{5/2}$) B.E. was observed at 280 eV which is in good agreement with the B.E. of Ru($3d_{5/2}$) in Ru metal (figure 10c). Thus, this result also confirms that in Ru ion substituted CeO_2, Ru is in 4+ oxidation state.

Ce (3d) spectra of freshly prepared and spent catalyst after WGS reaction are shown in figures 11 (a, b) respectively. Ce^{4+}($3d_{5/2}$) main peak at 882.7 eV along with satellite peaks at 6.4 and 16 eV below the main peak are characteristic of Ce^{4+} ion in CeO_2.[30] In Ce_2O_3, Ce^{3+} (3d) peaks were observed between Ce^{4+}($3d_{5/2}$) main peak and its first satellite peak. Ce^{3+} is characterized by Ce($3d_{5/2}$) main peak at 883.3 eV along with an intense satellite at 887.1 eV.[30] Thus filling of the valley between Ce^{4+}($3d_{5/2}$) main peak at 882.7 eV and its satellite at 889.1 eV confirms that Ce is in mixed valent (+4, +3) state in both as prepared and spent catalyst ($Ce_{0.95}Ru_{0.05}O_{2-\delta}$). Almost 20% Ce was observed in +3 state in spent catalyst where as only ~ 6% Ce^{3+} ion was present in as prepared catalysts. However in case of 5 atom% Ru metal impregnated on CeO_2 sample, Ce was found almost in 4+ oxidation state (figure 11c). Thus

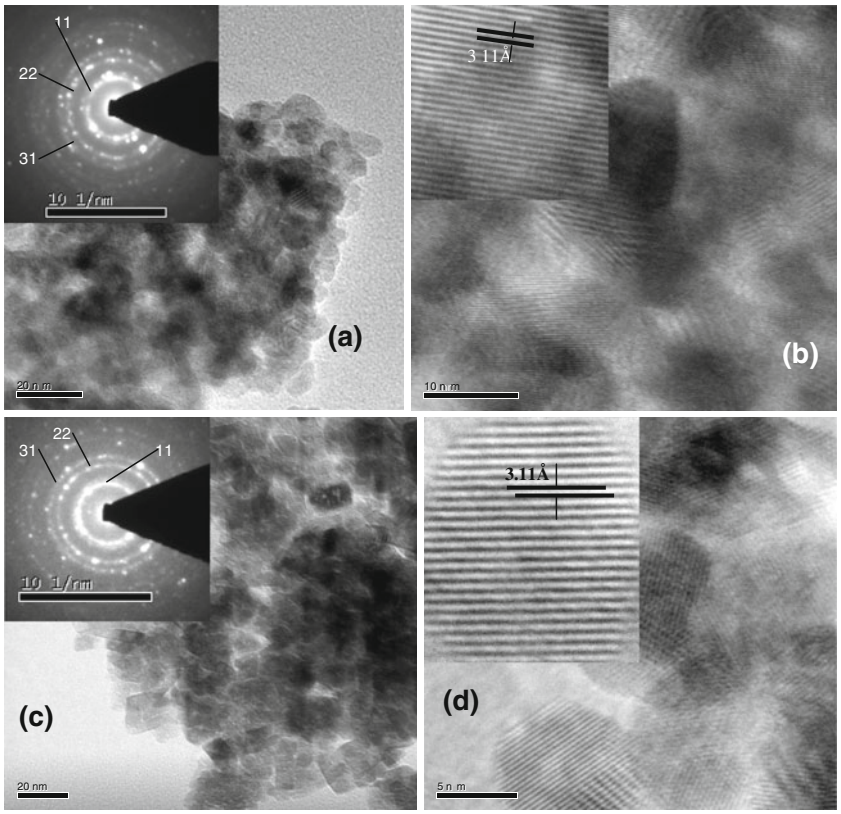

Figure 9. Bright field image and (**b**) HRTEM image of $Ce_{0.95}Ru_{0.05}O_{2-\delta}$ crystallites after 100 h of on/off WGS reaction. Inset of (**a**) and (**b**) shows indexed electron diffraction pattern and enlarged view of lattice fringes of spent $Ce_{0.95}Ru_{0.05}O_{2-\delta}$ catalyst respectively. (**c**) Bright Field image, (**d**) HRTEM image of freshly prepared $Ce_{0.95}Ru_{0.05}O_{2-\delta}$ and inset of (**c**) and (**d**) shows indexed electron diffraction pattern and enlarged view of lattice fringes of as prepared $Ce_{0.95}Ru_{0.05}O_{2-\delta}$.

small amount of Ce^{4+} reduction occurs after 100 h of on/off WGS cycle. Thus formula of active catalyst after 100 h of on/off WGS reaction cycle can be written as $Ce_{0.95}Ru_{0.05}O_{1.9}$ ($Ce_{0.75}{}^{4+}Ce_{0.2}{}^{3+}Ru_{0.05}{}^{4+}O_{1.9}$).

Relative surface concentration of Ru and Ce in $Ce_{0.95}Ru_{0.05}O_{2-\delta}$ catalyst (both as prepared and spent) was calculated from the formula:[31]

$$\text{Relative concentration } C_M = (I_M/\lambda_M\sigma_M D_M)/\Sigma(I_M/\lambda_M\sigma_M D_M), \quad (9)$$

where I_M is the integrated intensity of the core levels (M = Ce(3d) and Ru(3d)), σ_M is the photo-ionization cross section, λ_M is the mean escape depths of the respective photoelectrons, and geometric factor (D_M) is 1 for the instrument. The photo-ionization cross-section values were taken from Scofield's data[32] and mean escape depths were taken from Penn's data.[33] Indeed Ce and Ru were found in the ratio of ~ 0.94: 0.06 both in as prepared and spent catalyst. This is close to the nominal composition of Ru and Ce in $Ce_{0.95}Ru_{0.05}O_{2-\delta}$. Therefore, surface concentration of Ru in spent catalyst is almost same to the as prepared catalyst. This confirms that the segregation/separation of Ru ion does not occur under long duration of on/off WGS reaction cycle.

Coke and carbonate formation is considered as one of the prime reasons for deactivation of ceria based catalysts.[13–15,22,34] To see if carbon/coke is formed during the WGS reaction, the ratio of total intensity of C(1 s) and Ru(3d) was calculated for both as prepared and spent catalyst. Ru(3d) to C(1 s) intensity ratio in the catalyst before and after reaction (spent catalyst) remained same (figures 10 (a, b)). Thus no coke or C formation occurred over the catalyst surface. Surface carbonate is characterized by C(1 s) peaks at ~ 288–289 eV.[13–15,22,34] $Ru(3d_{3/2})$ peak also observed near to 285 eV. Thus if any surface carbonate would have formed over the catalyst under WGS reaction, there should have been an increase in $Ru(3d_{3/2})$ peak intensity in spent catalyst compared to freshly prepared catalyst. But $Ru(3d_{5/2})$ to $Ru(3d_{3/2})$ ratio also remained unchanged and also no

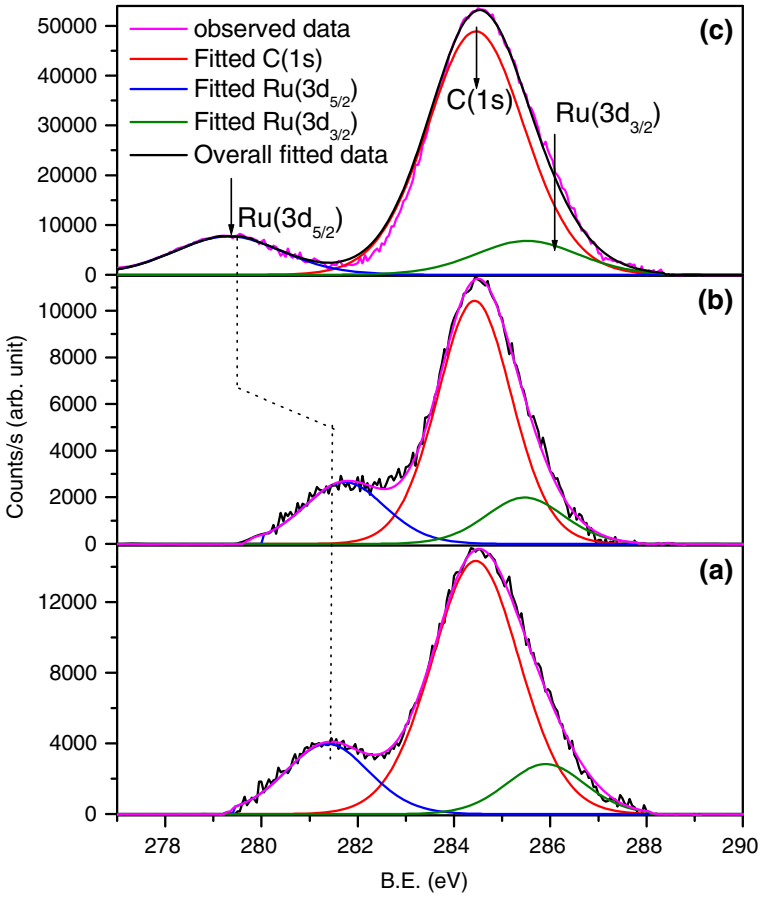

Figure 10. C(1s) + Ru(3d) XPS of $Ce_{0.95}Ru_{0.05}O_{2-\delta}$ (**a**) freshly prepared and (**b**) spent catalyst after 100 h of on/off WGS reaction. (**c**) C(1s) + Ru(3d) XPS of 5 atom% Ru metal impregnated on CeO_2.

peaks were observed close to 288 eV in XPS spectra. Thus surface carbonate formation does not occur over this catalyst during 100 h of on/off WGS reaction.

FT-IR spectra of both freshly prepared and spent catalyst are shown in figure 12. Carbonate (CO_3^{2-}) ions are characterized by characteristic peak for double degenerate stretching mode at $\sim 1417\,cm^{-1}$ and C=O stretching peaks at 1084 and 713 cm^{-1} in $CaCO_3$ (calcite)[35] and at 1450 cm^{-1} in CO_3^{2-} adsorbed on Pt metal.[36] Formate ion also shows stretching at 1321 cm^{-1} and 1565 cm^{-1}.[37] No peaks corresponding to carbonate and formate ions were observed in the FT-IR spectra of the spent catalyst. Thus absence of carbonate formation over the surface of $Ce_{0.95}Ru_{0.05}O_{2-\delta}$ catalyst was confirmed by FT-IR study.

Because of the high acidity of Ru^{4+} ion, carbonate formation does not occur over this catalyst. According to Fajan's rule,[38] acidity of metal ion increases with increase in charge/size ratio. The charge/size ratio of Ru^{4+} ion is 64. Absorption of acidic CO_2 over such a high acidic Ru^{4+} ion is not expected to form carbonate and formate species. Thus due to absence of carbonate and formate formation and absence of segregation of Ru^{4+} ion or separation of Ru from the catalyst, there was no deactivation in WGS activity of the catalyst.

However much higher WGS reaction activity was shown by the catalyst and equilibrium of reaction (1) is shifted towards right side. Almost 100% CO to CO_2 was observed with 100% H_2 selectivity was observed with this $Ce_{1-x}Ru_xO_{2-\delta}$ (x = 0.02 and 0.05) catalyst and complete conversion is also retained even at higher temperature (up to 500°C). The reason for this seems to be high adsorption propensity of CO on Ru^{4+} ion and easy extraction of oxygen from lattice to form CO_2. Activation of lattice oxygen in $Ce_{0.95}Ru_{0.05}O_{2-\delta}$ and utilization of high OSC for CO oxidation was presented in earlier report.[24] So in the first step of WGS reaction, CO is oxidized to CO_2 by lattice oxygen and reaction can be given as:

$$Ce_{0.95}Ru_{0.05}O_{1.97} + \delta CO \rightarrow Ce_{0.95}Ru_{0.05}O_{1.97-\delta} + \delta CO_2. \quad (10)$$

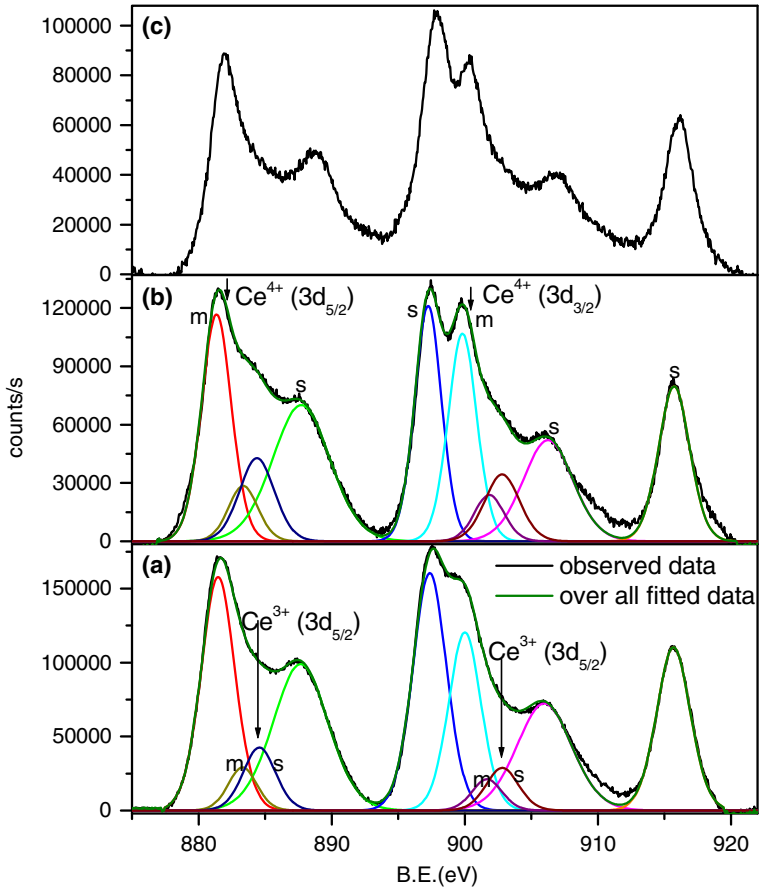

Figure 11. Ce(3d) XPS of $Ce_{0.95}Ru_{0.05}O_{2-\delta}$ (**a**) freshly prepared and (**b**) spent catalyst after 100 h of on/off WGS reaction. (**c**) Ce(3d) XPS of 5 atom% Ru metal impregnated on CeO_2.

This step creates oxide ion vacancy in the catalyst lattice and H_2O can be adsorbed on lattice oxygen vacancy sites. Catalyst lattice can be regenerated by releasing H_2 and reaction can be written as:

$$Ce_{0.95}Ru_{0.05}O_{1.97-\delta} + \delta H_2O \rightarrow Ce_{0.95}Ru_{0.05}O_{1.97} + \delta H_2. \quad (11)$$

In an independent experiment, this proposition was tested. First, CO was passed over 200 mg of the catalyst at 120°C and ~ 0.2 mol [O]/mol of compound was utilized to form CO_2 by CO oxidation in 50 minutes. After that H_2O vapors were passed at the same temperature over the catalyst and H_2 was generated in this process. This result justifies the mechanism proposed above in equations 10 and 11.

Since WGS reaction (equation 1) is a reversible and slightly exothermic reaction, complete conversion is not expected because reverse WGS reaction ($CO_2 + H_2 \leftrightarrow CO + H_2O$) occurs at higher temperatures. But for occurrence of the reverse reaction, CO_2 must be adsorbed on the catalyst and it should dissociate. Since Ru^{4+} ion is highly acidic, adsorption of acidic CO_2 over the catalyst is inhibited. This seems to be the reason why equilibrium is shifted towards right side and nearly 100% CO conversion to CO_2 was observed with 100% H_2 selectivity with this $Ce_{0.95}Ru_{0.05}O_{2-\delta}$ catalyst even up to 500°C. However in presence of excess H_2 and CO_2, lesser conversion was observed at same temperature with the catalyst as shown in figures 6 (a, b).

To confirm this proposition, reverse WGS reaction was carried out both in presence and absence of externally fed H_2O gas. First, reaction was carried out with gas composition 5 cc/min CO_2, 5 cc/min H_2 and 30 cc/min H_2O balance in N_2 keeping total flow 130 cc/min over 200 mg of catalyst. CO was not formed in the reaction even up to 600°C and also there is no measurable decrease in concentration of CO_2 and H_2 up to 600°C (figure 13a). Reaction was also carried out with gas composition 5 cc/min CO_2, and 5 cc/min H_2 balance in N_2 (in absence of feed H_2O) keeping total flow 130 cc/min over 200 mg of catalyst (figure 13b). No reaction was occurred up to 250°C and above this

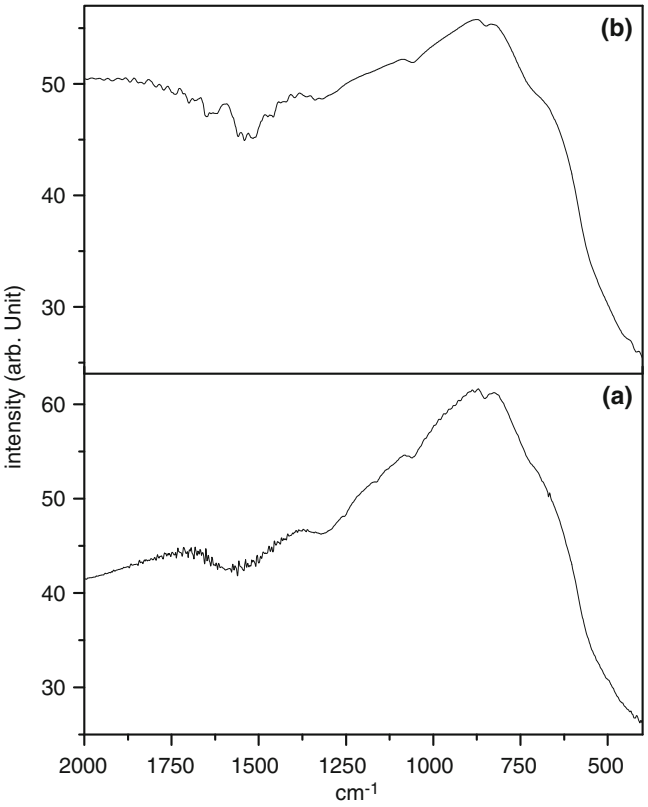

Figure 12. FT-IR spectra of (**a**) spent $Ce_{0.95}Ru_{0.05}O_{2-\delta}$ catalyst after 100 h of time scale on/off WGS reaction and (**b**) freshly prepared $Ce_{0.95}Ru_{0.05}O_{2-\delta}$ catalyst before WGS reaction.

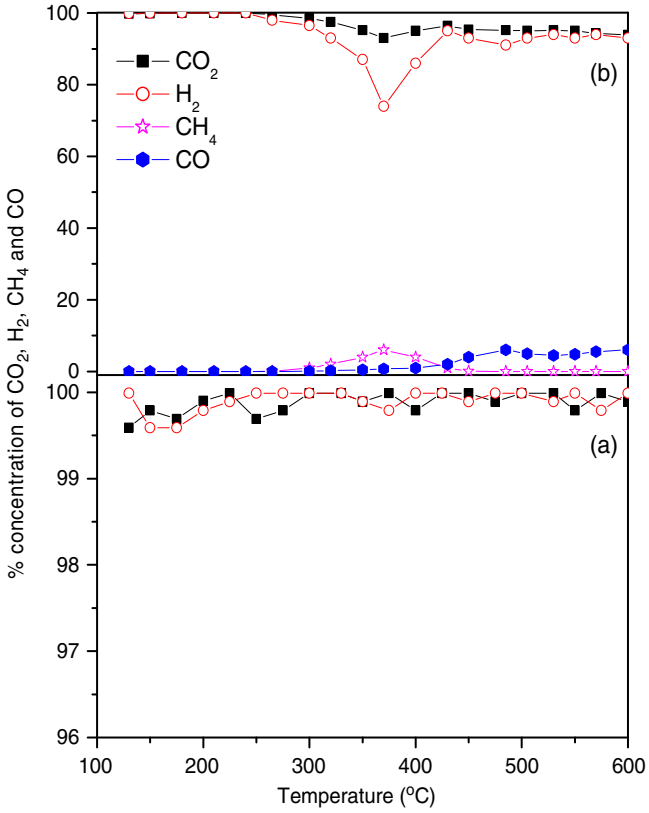

Figure 13. (**a**) % CO_2 and H_2 concentration plot as a function of temperature in reverse WGS reaction with gas composition 5 cc/min CO_2, 5 cc/min H_2 and 30 cc/min H_2O balance in N_2 (total flow, 130 cc/min) over 200 mg of $Ce_{0.95}Ru_{0.05}O_{2-\delta}$ catalyst. (**b**) % CO, CO_2, H_2 and CH_4 concentration in function of temperature in the reverse WGS reaction with gas composition 5 cc/min CO_2 and 5 cc/min H_2 balance in N_2 (total flow, 130 cc/min).

temperature, methane formation was observed in the temperature range of 265°C to 450°C. CO formation was also observed over 400°C. For example at 500°C, ~ 5% CO_2 is converted to CO in the reverse WGS reaction. This confirms that over this catalyst, reverse WGS reaction was occurring in presence of high volume of externally fed H_2O vapor. However both methane and CO formation was observed with the catalyst in absence of externally fed H_2O vapor. That is why nearly 100% CO conversion to CO_2 was observed with the Ru^{4+} ion substituted CeO_2 viz. $Ce_{1-x}Ru_xO_{2-\delta}$ (x = 0.02 and 0.05) catalyst even at 500°C.

The activity of this catalyst is due to substituted Ru^{4+} ion are in CeO_2 lattice because with 5 atom% Ru metal impregnated on CeO_2 catalyst, CO conversion decreased as well as methane formation was also observed at higher temperature. For example with 5 atom% Ru metal impregnated on CeO_2 catalyst at 500°C, ~ 97% CO conversion to CO_2 and CH4 was observed and ~ 3% CO was remained unreacted. Thus due to occurrence of reverse WGS reaction with Ru metal impregnated on CeO_2 catalyst, complete conversion of CO is not achieved at higher temperature. Thus only with Ru^{4+} ion substituted in CeO_2, $Ce_{1-x}Ru_xO_{2-\delta}$ catalyst almost complete conversion of CO to CO_2 is observed with 100% H_2 selectivity even up to 500°C.

4. Conclusions

$Ce_{0.95}Ru_{0.05}O_{2-\delta}$ nanocrystallites showed superior WGS reaction activity in terms of low activation energy (12.1 kcal/mol) and high conversion rates (20.5 μmol.g^{-1}.s^{-1}) at low temperature (275°C) compared to other composition namely $Ce_{0.98}Ru_{0.02}O_{2-\delta}$ and $Ce_{0.9}Ru_{0.1}O_{2-\delta}$. 100% H_2 selectivity was observed in WGS reaction with this catalyst and no trace of CH_4, CH_3OH, H_2CO and other hydrocarbon formation were observed over this catalyst. Even in presence of external/feed H_2 and CO_2 gas, almost complete conversion of CO to CO_2 with 100% H_2 selectivity was observed

in the temperature range 305–385°C. Deactivation of catalyst was not observed in on/off WGS reaction cycles and catalyst is highly stable in WGS reaction condition. Further sintering of noble metal (Ru) or active sites was avoided in this catalyst as Ru is present in ionic form (Ru^{4+}) in $Ce_{1-x}Ru_xO_{2-\delta}$ catalyst and due to highly acidic nature of Ru^{4+} ion, surface carbonate formation was also inhibited.

Acknowledgements

Authors thank Indian Council of Agricultural Research (ICAR) and Department of Science and Technology (DST), Govt. of India for financial support. Authors also thank Amit Mondal and Sharad Kumar of Nano centre, Indian Institute of Science Bangalore for recording TEM.

References

1. Taylor C F 1985 *Internal-combustion engine in theory and practice* - Vol. 1. (Cambridge: MIT Press). pp. 46 (ISBN: 0–262–70027–1)
2. *Wood gas as engine fuel*, M-38, Food and Agriculture Organization of the United Nations, Via delle Terme di Caracalla, 00100 Rome, Italy. (1986) (ISBN: 92–5–102436–7)
3. Lund C R F 2002 *Final Report to the United States Department of Energy* (DOE) Award No.: DE Aug 2002: FG2699–FT40590
4. Bunluesin T, Gorte R J and Graham G W 1998 *Appl. Catal. B* **15** 107
5. Qi X and Flytzani-Stephanopoulos M 2004 *Ind. Eng. Chem. Res.* **43** 3055
6. Ghenciu A F 2002 *Curr. Opin. Solid State Mater. Sci.* **6** 389
7. Amadeo N E and Laborde M A 1995 *Int. J. Hydrogen Energy* **20** 949
8. Fu Q, Saltsburg H and Flytzani-Stephanopoulos M 2003 *Science* **301** 935
9. Yeung C M Y, Meunier F, Burch R, Thompsett D and Tsang S C 2006 *J. Phys. Chem. B* **110** 8540
10. Phatak A A, Koryabkina N, Rai S, Ratts J L, Ruettinger W, Farrauto R J, Blau G E, Delgass W N and Ribeiro F H 2007 *Catal. Today* **123** 224
11. De Farias D A M, Bargiela P, Rocha M D G C, Fraga M A 2008 *J. Catal.* **260** 93
12. Si R and Flytzani-Stephanopoulos M 2008 *Angew. Chem., Int. Ed.* **47** 2884
13. Deng W and Flytzani-Stephanopoulos M 2006 *Angew. Chem., Int. Ed.* **45** 2285
14. Liu X, Ruettinger W, Xu X and Farrauto R 2005 *Appl. Catal. B* **56** 69
15. Ruettinger W, Liu X and Farrauto R 2006 *Appl. Catal. B* **65** 135
16. Azzam K G, Babich I V, Seshan K and Lefferts L 2007 *J. Catal.* **251** 153
17. Panagiotopoulou P, Christodoulakis A, Kondarides D I and Boghosian S 2006 *J. Catal.* **240** 114
18. Azzam K G, Babich I V, Seshan K and Lefferts L 2008 *Appl. Catal. A* **338** 66
19. González I D, Navarro R M, Lvarez-Galván M C A, Rosa F and Fierro J L G 2008 *Catal. Commun.* **9** 1759
20. Zalc J M, Sokolovskii V and Loffler D G 2002 *J. Catal.* **206** 169
21. Zhu X, Hoang T, Lobban L L and Mallinson R G 2009 *Catal. Lett.* **129** 35
22. Sharma S, Deshpande P A, Hegde M S and Giridhar M 2009 *Ind. Eng. Chem. Res.* **48** 6535
23. Gupta A and Hegde M S 2010 *Appl. Catal. B* **99** 279
24. Singh P and Hegde M S 2009 *Chem. Mater.* **21** 3337
25. Roisnel T and Rodríguez-Carvajal 2001 *J. Mater. Sci. Forum* **118** 378
26. Moe J M 1962 *Chem. Eng. Pro.* **58** 33
27. Kim K S and Winogard N 1974 *J. Catal.* **35** 66
28. Sakurai T, Hinatsu Y, Takahashi A and Fujisawa G 1985 *J. Phys. Chem.* **89** 1892
29. Rogers D B, Shannon R D, Slight A W and Gilson J 1969 *Inorg. Chem.* **8** 841
30. Kotani A, Ogasawara H 1992 *J. Electron Spectrosc. Relat. Phenom.* **60** 257
31. Powell C J and Larson P E 1978 *Appl. Surf. Sci.* **1** 186
32. Scofield J H 1976 *J. Electron Spectrosc. Relat. Phenom.* **8** 129
33. Penn D R 1976 *J. Electron Spectrosc. Relat. Phenom.* **9** 29
34. Ranga Rao G and Nozoye H 2003 *Surface Review and Letters.* **10** 917
35. Shivkumara C, Singh P, Gupta A and Hegde M S 2006 *Mater. Res. Bull.* **41** 1455
36. Iwasita T, Rodes A and Pastor E 1995 *J. Electroanalytical Chem.* **383** 181
37. Yang Y, Mims C A, Disselkamp R S, Peden C H F and Campbell C T 2009 *Top. Catal.* **52** 1440
38. Huheey J E 1983 *Principles of structures and reactivity in Inorganic Chemistry*, 3rd edn, Harper & Row (New York:Wiley) pp. 129